Rheol Acta (2011) 50:869–879
DOI 10.1007/s00397-010-0494-1

ORIGINAL CONTRIBUTION

Extensional rheology of human saliva

Simon J. Haward · Jeff A. Odell · Monica Berry · Tim Hall

Received: 9 June 2010 / Revised: 24 September 2010 / Accepted: 30 September 2010 / Published online: 24 October 2010

Abstract We have developed an oscillatory cross-slot extensional rheometer capable of performing measurements with unprecedentedly small volumes of test fluids (∼10–100 μL). This provides the possibility of studying exotic and precious or scarce bio-fluids, such as synovial fluid. To test our system, we have looked at a relatively abundant and accessible biological fluid, namely human saliva; a complex aqueous mixture of high molecular weight mucin molecules and other components. The results represent our first attempts to by this technique and as yet we have only sampled a small dataset. However, we believe we have produced the first successful quantitative measurements of extensional viscosity, Trouton ratio, and flow-induced birefringence made on saliva samples. The results significantly add to the scant literature on saliva rheology, especially in extension, and demonstrate the important role of saliva extensibility in relation to function.

This paper was presented at the 6th Annual European Rheology Conference, April 7–9, 2010, in Göteborg, Sweden.

S. J. Haward · J. A. Odell
H.H. Wills Physics Laboratory, University of Bristol, Tyndall Avenue, Bristol BS8 1TL, UK

M. Berry · T. Hall
University of Bristol Mucin Research Group, Bristol Royal Infirmary, Bristol BS2 8HW, UK

S. J. Haward (✉)
Department of Mechanical Engineering, Massachusetts Institute of Technology, 77 Massachusetts Avenue, Cambridge, MA 02139, USA
e-mail: shaward@MIT.EDU

Keywords Birefringence · Flow-induced orientation · Viscometry · Extensional flow · Saliva · Mucin

Introduction

Conventional rheology, for example in a cone and plate rotational rheometer, can measure the shear properties of polymeric liquids. However, many real flows, including those which are biologically relevant, are complex and can include both shear and extensional components. Extensional flows can significantly stretch macromolecules, providing orders of magnitude increases in elastic forces and extensional viscosity. Hence, measuring the extensional properties of a polymer solution is essential in order to fully characterize its rheological behavior in a real flow situation.

The rheology of complex polymeric biological fluids is vital to the correct functioning of many processes in the body. Examples of biological flows where extensional components are likely to play a key role include blood circulation (Lacombe and Essabbah 1981), synovial fluid function in the joints (Backus et al. 2002), and flows of mucus in the airways, tears in the eyes, and saliva in the mouth (Stokes and Davies 2007; Zussman et al. 2007). Drastically altered rheology of these fluids occurs (and may in some cases be a causal factor) in sickle cell anemia, osteoarthritis, chronic pulmonary conditions like cystic fibrosis (Rubin 2007), as well as dry eye and mouth syndromes like Sjögren's and oral mucositis (Rossi et al. 2010). Sjögren's syndrome is an autoimmune disease that results in the destruction of the exocrine glands which produce tears and saliva. Therefore, understanding the different extensional rheology of healthy and unhealthy fluids in relation to their

function could provide important benefits in terms of developing novel treatments and therapies and potential diagnostic applications.

In this paper, we present preliminary results obtained with a modified extensional flow oscillatory rheometer (EFOR, Odell and Carrington 2006; Haward et al. 2010a, b). The new version of the apparatus allows extensional viscosity and flow-induced birefringence measurements to be made on extremely small test sample volumes. Flow-induced birefringence indicates orientation of macromolecules as they become anisotropic in flow. We envision this development to be particularly useful for studies of scarce or precious biological fluids, such as comparing the rheology of healthy synovial fluid with the degraded synovial fluid from osteoarthritis patients. However, we have performed initial experiments to demonstrate the potential of the technique using a plentiful and accessible biological fluid; normal healthy adult human saliva.

The EFOR is a stagnation point extensional flow device based on the cross-slot of Scrivener et al. (1979). A stagnation point is a singularity in a flow field where the flow velocity is zero but the velocity gradient, or strain rate ($\dot{\varepsilon}$), is finite and can be large. Therefore macromolecules can become trapped at the stagnation point for, in principle, infinite time, where they can accumulate strain on condition that $\dot{\varepsilon} > \sim 1/\tau$, where τ is the molecular relaxation time. Studies of flow-induced birefringence with model polymeric systems such as dilute atactic polystyrene in decalin or dioctyl phthalate have shown that polymer molecules can become significantly extended under such conditions (e.g., Carrington et al. 1997a, b; Odell and Carrington 2006; Haward et al. 2010a). In these studies, when $\dot{\varepsilon}$ exceeded $1/\tau$, long localized strands of highly stretched molecules (visible as birefringent strands) were observed extending downstream from the stagnation point. Associated with this was a significant increase in the extensional viscosity, as determined from measurements of the pressure drop across the apparatus. Direct microscopic observation of fluorescently labeled DNA molecules at the stagnation point of a cross-slot has also shown that significant molecular strain can be accumulated (Perkins et al. 1997; Smith and Chu 1998).

Saliva is a mucous secretion that coats the surface of the oral cavity and is an aqueous mixture of mucins, lipids, and other proteins and bioactive molecules (Beeley 1993; Helmerhorst and Oppenheim 2007). Its rheology is important for numerous functions such as mastication, bolus formation, and swallowing (Pedersen et al. 2002). There have been a small number of studies focusing on the shear rheology of saliva using cone and plate rheometers. Early studies appeared to show that saliva is gel like, due to the existence of a yield stress and shear thinning (e.g., Davis 1971; Schwarz 1987); however, Waterman et al. (1988) later demonstrated that the apparent yield stress was likely to be an artifact originating from the adsorption of a protein layer at the air–liquid interface between the edges of the rheometer plates. Similar issues have also been encountered in rheometric studies with various other protein solutions, such as bovine serum albumin (see e.g., Sharma et al. 2010). Van der Reijden et al. (1993a, b) overcame this problem by utilizing a Vilastic capillary rheometer to study saliva. They observed different viscoelastic properties for the saliva secreted from different glands within the oral cavity, which they explained as being due to the saliva containing mucins of different conformation, molecular weight, and concentration. Other studies have focused on how stimuli can affect saliva properties. Briedis et al. (1980) reported that saliva viscosity could increase significantly immediately after eating, drinking coffee, or if under stress, although they found no significant variation of saliva viscosity with donor age or sex. However, the results of Briedis et al. are also likely to have been influenced by the adsorption of an interfacial protein layer. Stokes and Davies (2007) used a cone and plate rheometer but avoided the problems associated with the air–liquid interface by applying a sodium dodecyl sulfate (SDS) solution around the edges of the rheometer plates. They found the saliva to be shear thinning and also that the viscosity and viscoelasticity of saliva depended greatly on the method of stimulation (acid or mechanical). With acid-stimulated saliva they found a ratio of first normal stress difference to shear stress of order 100, for shear rates $>100\ s^{-1}$, indicating that elastic properties may dominate the behavior of saliva in flow. The rheology of the saliva was well described by a multi-mode Maxwell model with a longest relaxation time of about 1 s and two shorter relaxation modes. However, using a finitely extensible non-linear elastic (FENE-P) dumbbell model, an extremely long relaxation time of 76.2 s was required to fit the data for citric acid stimulated saliva. This time scale was longer than the inverse of the lowest frequency accessible by the rheometer but its requirement for the data fitting indicates the likely existence of an extremely long relaxation mode in the saliva. This is considered to reflect the presence of extremely high molecular weight mucin molecules. The results of Stokes and Davies strongly suggest the importance of the extensional properties of saliva, which is expected to provide a protective function within the oral cavity, such as formation the acquired enamel pellicle, as well as influencing food and beverage processing, mouth-feel and texture per-

ception, and lubricating the mouth for mastication and speech articulation.

Apart from the very early efforts of Dewar and Parfitt (1954) to study flow elasticity and "spinnbarkeit" (or spinnability) of saliva using equipment based on the designs of Clift and Scott-Blair (1945) and Erbring (1936), we are aware of only one published study reporting specifically on the extensional rheology of saliva, namely that of Zussman et al. (2007). They used a filament stretching type rheometer to measure different relaxation times for saliva obtained from the different salivary glands. In addition, they found that the relaxation time of unstimulated whole saliva increased by 54% (from ~2.24 to 3.45 ms) between subjects in their early 1920s and those in their 1970s, leading to the suggestion that changes in saliva viscoelasticity with age may be clinically important and may relate to an increased incidence of oral cavities in the elderly.

The present study therefore significantly adds to what is currently a very limited set of literature data on the extensional flow of saliva, and provides totally new quantitative information on the extensional viscosity and flow-induced birefringence in saliva.

Experimental

Apparatus

A schematic diagram of the EFOR system is shown in Fig. 1. The apparatus is essentially as described in Odell and Carrington (2006). Fluid is pumped into one pair of opposing channels and out of the second pair, resulting in a stagnation point at the center of the cross. The piezoelectric micro-pumps are driven by applying oscillating triangular voltage profiles (corrected for piezo hysteresis) of amplitude, $V/2$, and period, T, across them. This results in a linear displacement of each pump and hence a constant volume flow rate Q ($\propto V/T$) through each channel of the slot.

The superficial flow velocity, U, in each channel is given by:

$$U = \frac{Q}{dt} \tag{1}$$

Where d is the width of the channel and t is the depth of the channel. The nominal extensional strain rate at the stagnation point, $\dot{\varepsilon}$, is given by:

$$\dot{\varepsilon} = \frac{2U}{d} \tag{2}$$

The slots used in this study have a channel width of $d = 200$ μm and a depth of $t = 1$ mm, giving an aspect ratio of 5:1, and hence a reasonable approximation to 2D flow. The total length of each channel is $L = 1.2$ mm.

The major innovation for this work has been the addition of an injection point on one arm close to (~3.5 mm from) the center of the cross-slot, as shown in Fig. 2. This allows test fluid (saliva in this case) to be injected only into the cross, while the rest of the apparatus (i.e., pumps and pipes) is filled with a solvent. Approximately 30 ml of solvent was required to fill the

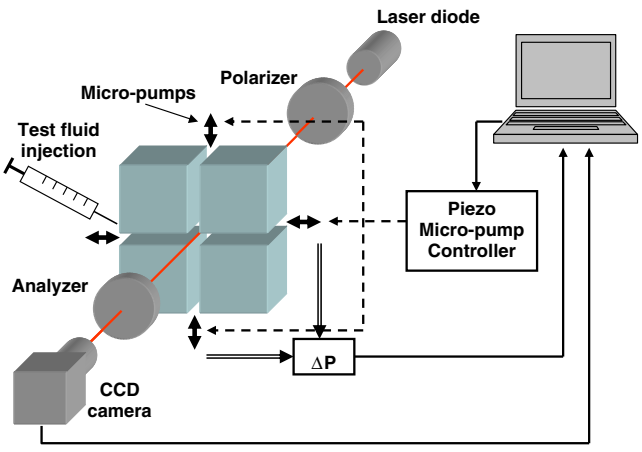

Fig. 1 Schematic diagram of the EFOR including micro-pump control, test fluid injection, pressure measurement, and optical line

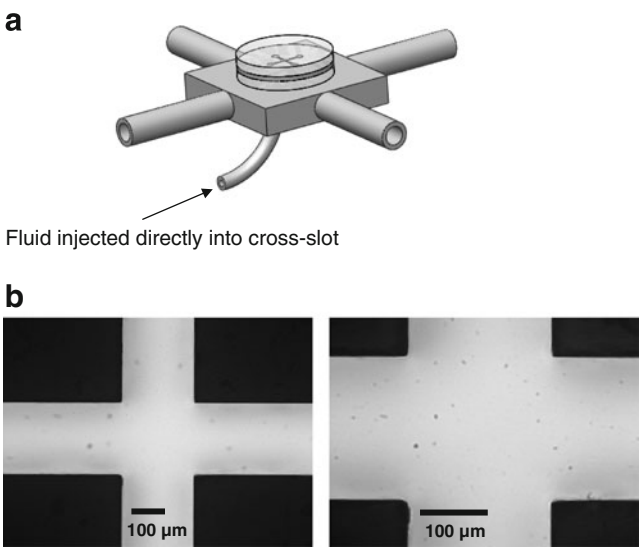

Fig. 2 **a** Schematic view of a cross-slot flow cell, showing the injection port. **b** Micrographs of the cross-slot (with 200-μm wide channels), which was fabricated from stainless steel by wire electrical discharge machining (wire EDM)

entire system. In the present experiments, we filled the apparatus with a phosphate-buffered saline solution, although subsequent tests showed that deionized water would have been equally suitable. By using the piezo pumps to draw fluid from the injection point into the cross, it was possible to use only the exact volume of test fluid required for a given experiment, as determined by the piezo voltage parameter, V. For example, for an operating voltage of $V = 100$ V (the maximum rating for the piezos), the pumped volume of fluid was ~40 μL in each pump (160 μL in total for all four pumps). Most experiments were conducted at lower voltages than this; V was generally varied between $10V < V < 90V$ and a proportional volume of saliva was required at each voltage. Calculations based on the injected volumes and the dimensions of the 5-ml syringe (with 12-mm inner diameter) used to inject the saliva samples into the cross-slot indicate that shear and extensional strain rates would have been $<10\ s^{-1}$ through the syringe. This is unlikely to have caused degradation of even the highest molecular weight mucins. There was of course inevitable mixing between the test fluid contained in the cross-slot and the surrounding solvent. However, tests with solutions of poly(ethylene oxide) showed that the mixing was slow compared with the time scale of an experiment, which typically only took ~5 s. Since it was easy to collect between 5 and 10 mL of saliva it was possible to make a relatively large initial injection into the cross-slot to significantly displace the surrounding solvent away from the active stagnation point region of the cross (note that the entire volume of the cross-slot was only $\sim 4 \times 10^{-6}$ mL). Subsequently, fresh saliva was injected following the acquisition of data at each strain rate, further displacing the solvent. Valves were employed to isolate the cross-slot containing the saliva test fluid from rest of the tubing to prevent mixing occurring in between the taking of test points. Since measurements were only made on fluid contained in the close vicinity of the stagnation point region (birefringence was measured at the stagnation point and the pressure drop was entirely dominated by the flow in the narrow channels of the cross) the measurements should not have been affected by the solvent in the tubing. This was confirmed by the tests described above.

The pressure difference, ΔP, in the cross-slots was measured as a function of strain rate across an inlet (entry) and an outlet (exit) channel using a Druck 200 kPa differential pressure sensor, as shown schematically in Fig. 1. The pressure ports were located ~50 cm apart in the tubing connecting the micro-pumps to the cross-slot entry/exit channels. By disconnecting two of the four micro-pumps and simply measuring the pressure drop for flow of liquid around a corner of the cross-slot (ΔP_{shear}), we could obtain a measure of the shear viscosity, η_{shear}, of the liquid. Neglecting the small perturbation resulting from the corner of the cross (e.g., Craven et al. 2010) and assuming Poiseuille flow in a rectangular channel of total length $2L$:

$$\eta_{\text{shear}} = \frac{d^2 \Delta P_{\text{shear}}}{24UL} \tag{3}$$

Results for η_{shear} obtained with Eq. 3 have previously been shown to agree closely with results from a conventional ARES rotational rheometer (Haward et al. 2010b).

By measuring the pressure drop with all four pumps running (ΔP_{total}), we could find the excess pressure drop due to the extensional part of the flow field. By assuming the extensional viscosity in the birefringent strand $\eta_{\text{ext}} >> \eta_{\text{shear}}$ and therefore dominated the excess pressure drop, we obtained a measure of the extensional viscosity of the fluid comprising the elastic strand thus:

$$\eta_{\text{ext}} = \frac{\Delta P_{\text{total}} - \Delta P_{\text{shear}}}{\dot{\varepsilon}} \times \frac{d}{w} \tag{4}$$

Where w is the width of the birefringent strand (full width at half maximum intensity).

The Trouton ratio, Tr, is defined by:

$$Tr = \frac{\eta_{\text{ext}}}{\eta_{\text{shear}}} \tag{5}$$

All data was captured after the pressure drop had reached a steady state. Under typical operating parameters this was achieved within ~0.1 s in a 2-s pumping cycle.

The optics used for birefringence observation and measurement are also shown in Fig. 1. The light source was a temperature stabilized 660-nm 60-mW fiber-coupled diode laser from Oz Optics. The polarizer and analyzer were initially crossed at ±45° to the direction of the channels of the cross-slot and a λ/4 plate was used to compensate for residual birefringence in the system in order to maximize the extinction. Subsequently, following the method of Riddiford and Jerrard (1970), the polarizer was uncrossed by a small amount (<3°) to allow a background signal through in order to increase the signal to noise ratio for birefringence detection. The CCD camera was a deeply cooled (−80°C), very low noise, high quantum efficiency (~60%), 14 bit, 1,000 × 1,000 pixel model from Andor Technology.

Saliva

Human whole saliva was collected from two healthy subjects, who will be referred to as 'M' and 'S'. Since

it has been shown that saliva properties can vary after consumption of food or drink and due to the method of stimulation (Briedis et al. 1980; Stokes and Davies 2007), the saliva in this study was collected early in the morning (at approximately 9:00 am) between 1 and 2 h after adequate oral hygiene and before any food or drink had been consumed. Following collection, the saliva was immediately transferred into 1.5-mL Eppendorf containers and centrifuged at 10,000×g for 5 min to remove any particulate matter, cells, and bacteria. Following the processing procedure, the samples were tested in the EFOR without delay. We initially followed the saliva collection procedures of Stokes and Davies (2007), i.e., tested whole unprocessed saliva samples collected after stimulation. However, although it was possible to measure the pressure drop from such samples in our apparatus (results presented later in Fig. 8), cells and other particulate matter interfered to such an extent with our optical set up that useful birefringence measurement (and even observation) was impossible. It was also a concern that such cells or particles could become trapped in the narrow channels of the cross-slot. Subsequently, it was decided that centrifugation of the saliva samples, which is a standard practice in many areas of saliva research (Schipper et al. 2007), was essential in our experiment.

The effect of centrifugation on the saliva samples was investigated using an m-VROC microfluidic rheometer (Rheosense Inc.), suggested by Sharma et al. (2010) as suitable for protein solutions in which adsorption of protein to the air/liquid interface may have a significant influence on standard cone and plate rheometry. The results are presented in Fig. 3 and demonstrate a notable difference in rheology between whole and centrifuged saliva samples. The whole saliva sample shows a significant degree of shear thinning over the shear rate range, with a viscosity of ~8 mPa s at the lowest shear rate and a reduction to ~2 mPa s at higher shear rates (the large error bars are due to the large variation in viscosity measured for different saliva samples). The results for the whole saliva are similar to the results of Stokes and Davies (2007) using an ARES cone and plate rheometer with the air–liquid interface protected by an SDS solution. The centrifuged saliva in Fig. 3 shows a near constant viscosity of ~1.5 mPa s, with perhaps a mild degree of shear thinning at high shear rates. The measured viscosity of water is shown in Fig. 3 for comparison. The different rheology of the saliva samples is almost certainly explained by the loss of some of the large macromolecular assemblies during centrifugation, although it should be noted that cryo-scanning electron microscopy studies of saliva samples have shown that extensive mucin networks remain intact after centrifugation (e.g., Schipper et al. 2007). Also, even after centrifugation our saliva samples still showed substantial elasticity in finger tests.

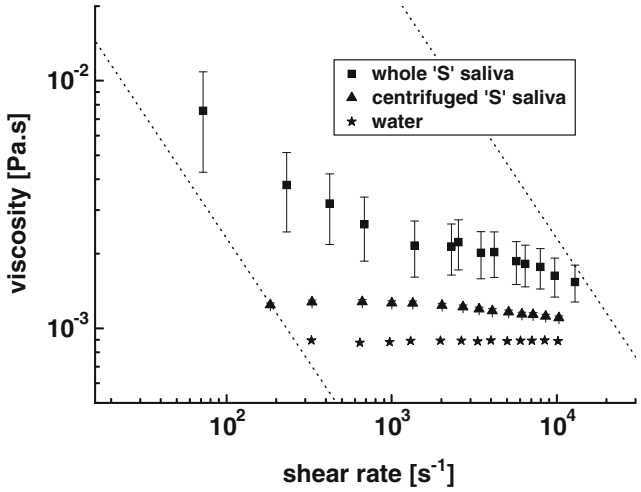

Fig. 3 The effect of centrifugation on the shear viscosity of saliva, measured using an m-VROC microfluidic rheometer. The *dotted lines* represent the lower and upper limits of the rheometer pressure sensor

Of all the components present in saliva, the gel-forming mucin MUC5B has by far the highest molecular weight, M_w, reaching up to 2–40 MDa (Thornton et al. 1999) and many micrometers in length (Kesimer et al. 2010). Another main salivary mucin component, MUC7, is monomeric with a molecular weight of ~150 kDa (Mehrotra et al. 1998), but can also self-aggregate, while MUC16, a mucin shed from the oral surface epithelial cells has $M_w \sim 2.5$ MDa (Hattrup and Gendler 2008). The concentrations of MUC5B and MUC7 in saliva have been reported as 233 μg/ml (0.0233 wt.%) and 133 μg/ml (0.0133 wt.%), respectively (Rayment et al. 2000). Therefore, due its higher molecular weight and concentration, we expect the MUC5B mucin to dominate the behavior of saliva in extensional flow. On the other hand, for the following reasons it is simplistic to consider saliva as simply a solution of MUC5B: (1) Raynal et al. (2002) have shown that even concentrated solutions of MUC5B do not fully replicate the gel-like properties of whole saliva, (2) the presence of other mucins such as MUC7 and MUC16 that can aggregate with each other and other molecular species, as suggested by their migration into agarose and NuPage gels, and (3) the presence of various lubricative and surface active molecules.

Mucins are very high molecular weight glycoconjugates consisting of a polypeptide backbone decorated by oligosaccharide side chains. Most are *O*-linked to

a serine (Ser) or threonine (Thr), and are arranged in dense patches along the peptide core. Regions of less dense *O*-glycosylation flank the central mucin domains, where *N*-linked glycans can be found (illustrated schematically in Fig. 4). Mucins dimerize early during biosynthesis, and polymerize further through disulfide bonds. Most mucins are linear polymers: MUC7 is an exception to the rule, and can be found in radial arrangements around a central moiety (Mehrotra et al. 1998). MUC16 is a cell surface-tethered mucin, whose large extracellular domain is shed into the saliva (Davies et al. 2007).

Thomsson et al. (2002) have conducted an extensive structural and chemical analysis of the MUC5B mucin. They found that the molecule consists of ~20 wt.% protein and ~80 wt.% carbohydrate. Of the protein component ~1/3 of the amino acid residues are either Ser or Thr. Using this information, we can make some inferences about the average nature of the mucin molecule. From the mass of protein in the mucin, we can calculate the approximate contour length, L, of the molecule (neglecting the short N- and C-terminal domains):

$$L = \frac{M_p}{m_{aa}} \times \ell_{aa} \sim \frac{0.2 \times M_w}{m_{aa}} \times \ell_{aa} \tag{6}$$

Where M_p is the mass of protein in the mucin molecule, m_{aa} is the average mass of a single amino acid residue (=135 Da), and ℓ_{aa} is the length of an amino acid residue (=0.38 nm).

The total number of amino acid residues is given by M_p/m_{aa}, hence the number of Ser and Thr residues is approximately one third of this value, $M_p/3 \times m_{aa}$. Using this, and the total mass of carbohydrate in the mucin molecule, $M_c = 0.8 \times M_w$, we can estimate the average mass of the oligosaccharide side chains, m_{os}:

$$m_{os} = M_c \times \frac{3 \times m_{aa}}{M_p} = 12\, m_{aa} \sim 1{,}600 \text{ Da} \tag{7}$$

This value of m_{os} corresponds to an average of ~8 monosaccharides per oligosaccharide side group. A schematic of the chemical structure is shown in Fig. 4c. It should be noted, however, that the oligosaccharides can be either linear or branched and can vary in length between one and ~20 sugar residues (Thomsson et al. 2002).

To our knowledge, the only estimate for the persistence length of mucin molecules comes from Round et al. (2002), who studied linear human ocular mucins using atomic force microscopy. Imaging analysis techniques were employed, along with a 2D projection of the worm-like chain model (Kratky and Porod 1949; Flory 1969), to determine the persistence length, $p = 36 \pm 3$ nm.

This persistence length is likely to be influenced by factors such as the pH and ionic strength of the solvent. However, on the assumption that salivary mucins will have a comparable persistence length to the ocular mucins studied by Round et al., we can use the worm-like chain model to estimate the root-mean-square end-to-end length of the mucins, $\langle r_0^2 \rangle^{1/2} = \sqrt{2pL}$, and the radius of gyration, $R_g = \langle r_0^2 \rangle^{1/2} / \sqrt{6}$. Given $\langle r_0^2 \rangle^{1/2}$ and L, the maximum strain to full stretch of the molecule is found to vary between $\sim 4 < L/\langle r_0^2 \rangle^{1/2} < \sim 17$ for mucin molecular weights between 2 MDa $< M_w <$ 40 MDa. As a comparison, flexible high molecular weight polymers in theta solvents may require strains of up to 100 or more to achieve full extension, see Carrington et al. (1997b). Using the value of R_g for the mucins, we can estimate the critical

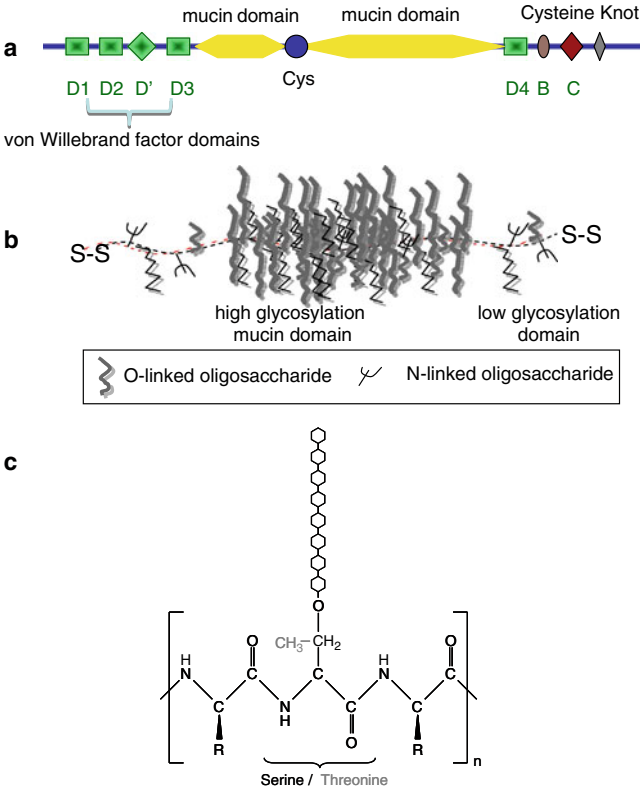

Fig. 4 Schematic of salivary mucin structure: **a** the entire mucin molecule, **b** close up of a mucin domain, **c** chemical structure of a typical repeat unit in the mucin domain, showing an *O*-linked oligosaccharide side-chain on the Ser/Thr residue

overlap concentration, c^*, for the MUC5B molecule in solution in saliva. Assuming a simple cubic packing of mucin molecules (Graessley 1980), the overlap concentration (in units of wt.%) is given by, $c^* = M_w/10{,}000 \times N_A \times (2\times R_g)^3$, where N_A is Avogadro's constant.

Based on the preceding analysis, Fig. 5 shows a plot of R_g and c^* as a function of the mucin molecular weight, over the expected molecular weight range for salivary mucins of 2 MDa $< M_w <$ 40 MDa (Thornton et al. 1999). Considering the assumptions made, especially regarding persistence length, the calculated values for R_g agree well with light scattering data obtained with MUC5B solutions (Sheehan et al. 1999). Figure 5 shows a reduction in the value of c^* from ~0.026 wt.% down to ~0.006 wt.% with increasing molecular weight. If the concentration of mucins in saliva is around 0.02 wt.% (Rayment et al. 2000), we therefore see that the MUC5B component of saliva probably exists in the semi-dilute, unentangled, concentration regime with $\sim 1 < c/c^* < \sim 4$ (Colby 2010). This is an interesting concentration range, since it is in the lower limit for which the mucins could possibly form a gel-like network. However, MUC5B is capable of forming extremely high molecular weight concatenated molecules through disulfide bonding, which could lower the value of c^* even further (Kesimer and Sheehan 2008). Also, this mucin is only one of many complex molecules present in saliva, which further complicates the preceding analysis. Nonetheless, it is instructive to have at least a crude picture of the molecular architecture, conformation, molecular weight, and concentration range of the molecules which are most likely to have the largest impact on saliva rheology.

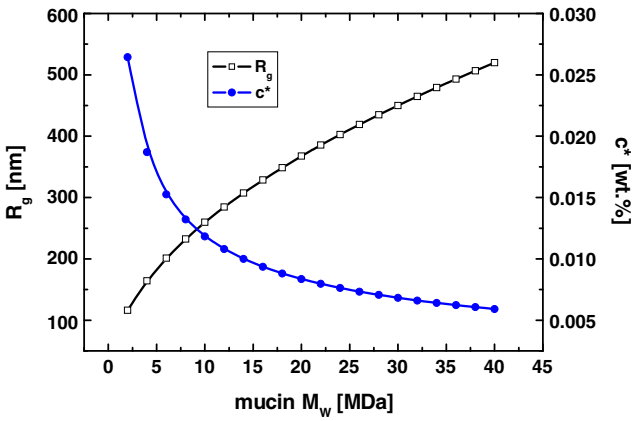

Fig. 5 Expected radius of gyration, R_g, and overlap concentration, c^*, as a function of MUC5B mucin molecular weight

Results

Figure 6 shows how the birefringence observed in the cross-slot with saliva collected from donors 'M' and 'S' varied over a range of strain rates. It should be noted that the intensity scale is non-linear, meaning that the intensity range of each image has been individually adjusted to give the best contrast of the birefringent strand in each case. Both saliva samples show broadly similar qualitative behavior. At low strain rates, the birefringent strand is quite narrow and localized along the flow axis passing through the stagnation point at the center of the cross. As the strain rate is increased the

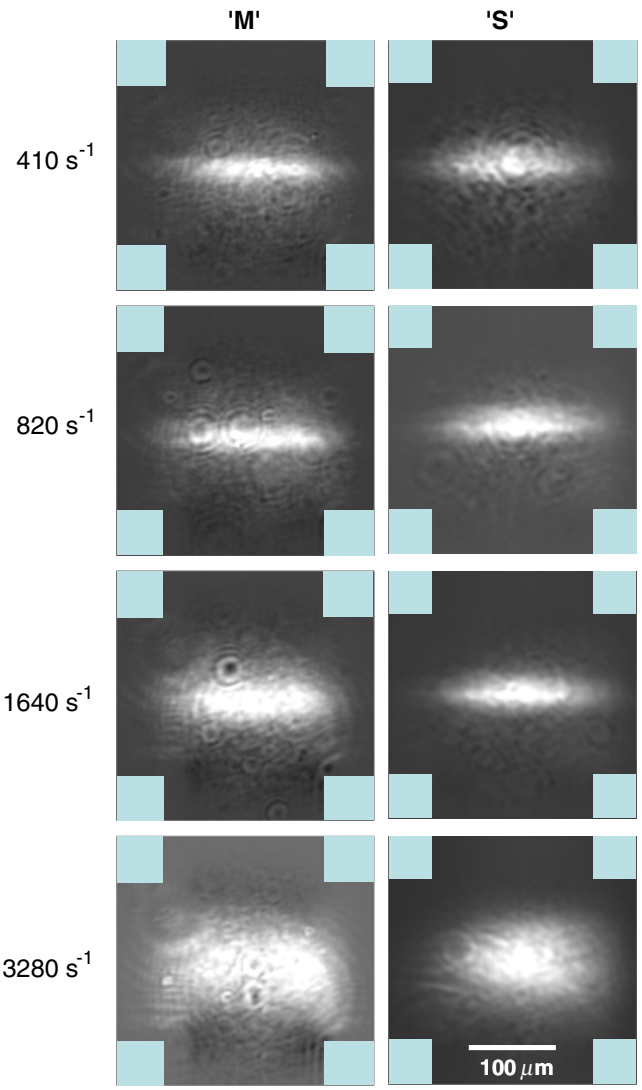

Fig. 6 Birefringence observed in centrifuged human saliva samples from subjects 'M' and 'S' at the strain rates indicated to the *left*. The intensity scale is non-linear. The positions of the cross-slot walls have been artificially superimposed for clarity

birefringent strand observed in sample 'M' gradually begins to broaden (e.g., at 1,640 s^{-1}) until we observe a wide band of birefringence across a significant portion of the width of the channels (e.g., at 3,280 s^{-1}).

In both the 'M' and 'S' saliva samples, birefringence was weakly detectable down to strain rates, $\dot{\varepsilon} \sim 200\,s^{-1}$ (photographic data not shown, but see Fig. 7), indicating a longest molecular relaxation time of $\tau = 1/\dot{\varepsilon}$ at least 5 ms, which is of a similar order to the value of 2.24 ms reported by Zussman et al. (2007) for unstimulated whole saliva in a filament stretching rheometer. However, these relaxation times are much lower than the values of 1 and 76.2 s reported by Stokes and Davies (2007), which in our case might be a result of centrifuging the samples and loss of macromolecules. As in the 'M' saliva sample, we also observe broadening of the birefringent strand with increasing strain rate in the 'S' sample, though delayed to slightly higher strain rate. Broadening of the birefringence in the cross-slot with strain rate is a feature that has been seen previously with semi-dilute polymer solutions (e.g., Keller et al. 1987; Haward et al. 2010b) where it has been attributed to entanglement networks, and in solutions of worm-like molecules, which can stretch at low strains and strain rates (Carrington et al. 1996). Here, the origin of the broadening is most likely attributed to the worm-like nature of the mucins, which are stiffened by the densely glycosylated sections. The very low strain to full stretch of the mucin molecules ($4 < L/\langle r_0^2 \rangle^{1/2} < 17$, depending on molecular weight) would allow them to become highly stretched and oriented even along streamlines that pass far from the stagnation point (given a sufficient volume flow rate).

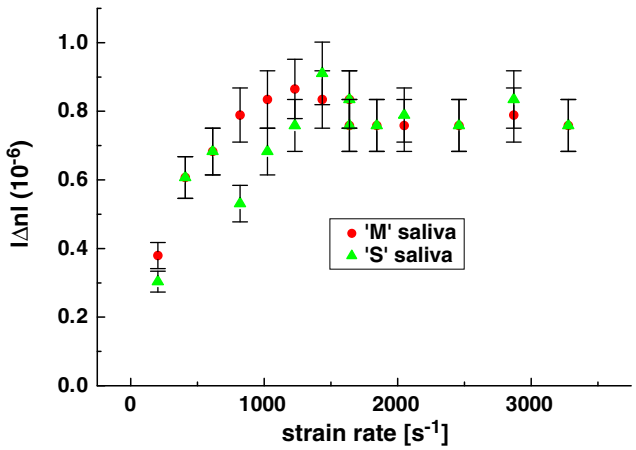

Fig. 7 Absolute values of the maximum measured birefringence as a function of strain rate for the centrifuged saliva samples in the cross-slot

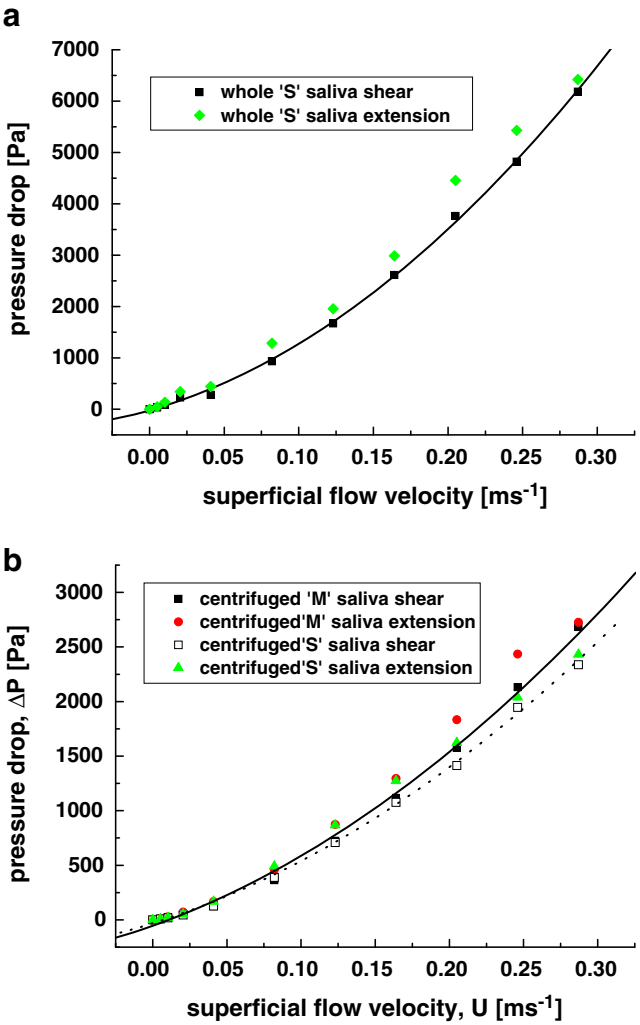

Fig. 8 Pressure drop measurements measured in both shear and extensional flow in the cross-slots with **a** whole saliva samples from subject 'S' and **b** centrifuged saliva samples from subjects 'M' and 'S'. The *solid and dotted lines* are quadratic fits to the shear flow data

Figure 7 shows the absolute value of the birefringence, $|\Delta n|$, measured at the stagnation point as a function of strain rate in the 'M' and 'S' saliva samples. Both show very similar behavior with the birefringence increasing from $\dot{\varepsilon} \sim 200\,s^{-1}$ up to a maximum value of $|\Delta n| \sim 0.8 \times 10^{-6}$ at $\dot{\varepsilon} \sim 1{,}200 - 1{,}500\,s^{-1}$, before a plateau. Due to the method employed to measure the birefringence (see Section "Experimental"), we are able to distinguish between molecules of positive and negative birefringence. Comparison of the birefringence observed in saliva samples with that observed in a synthetic polymer solution of known positive birefringence (an aqueous poly(ethylene oxide) solution) indicates that the mucins in saliva also have a positive birefringence. That is to say the mucin birefringence is

probably dominated by the orientation of the polypeptide backbones as opposed to the orthogonal oligosaccharide side chains.

Experiments by various authors with a variety of polymer solutions of different flexibility under different solvent conditions have shown that at high strain rates in cross-slot flow the molecular end-to-end distance, r, tends to a maximum of ~0.6–0.7 times the contour length, L (e.g., Perkins et al. (1997) with DNA solutions, Haward et al. (2010a) with aPS/DOP, and Haward et al. (2010b) with aqueous PEO). The model of Treloar (1975), based on the optical properties of strained networks, relates the ratio of r/L to the birefringence of the network via an approximation to the inverse Langevin function:

$$\frac{\Delta n}{\Delta n_0} = \frac{3}{5}\left(\frac{r}{L}\right)^2 + \frac{1}{5}\left(\frac{r}{L}\right)^4 + \frac{1}{5}\left(\frac{r}{L}\right)^6 \quad (8)$$

Where Δn_0 is the birefringence of a solution of fully stretched molecules.

Assuming the mucin molecules in the saliva also stretch to $r/L \sim 0.6$, we can use Eq. 8 to estimate $\Delta n_0 \sim 3 \times 10^{-6}$ for the centrifuged saliva samples. Further, assuming only a small proportion of the mucin is lost during centrifugation so that the mucin content in the saliva samples is close to 0.02 wt.% (Fox et al. 1985), we can estimate the maximum birefringence for a generalized solution of fully stretched salivary mucin molecules to be $\Delta n_0 = 0.015 \times c$, where c is the mucin concentration.

Figure 8 displays the pressure drop measured in the cross-slot for both shear and extensional flow. The whole saliva from subject 'S' (Fig. 8a) was collected by stimulation with 0.25% citric acid solution following (Stokes and Davies 2007). The centrifuged saliva samples from subjects 'M' and 'S' (Fig. 8b) were collected as described in the Section "Experimental". For all the samples the pressure drop in shear is well described by a quadratic in superficial flow velocity, indicating the presence of inertial effects in the flow; the Reynolds number is $1 < \mathrm{Re} < 50$. It is clear that for a given superficial flow velocity, U, there is a considerably lower pressure drop recorded in the centrifuged samples. Equation 3 can be used to calculate the shear viscosity at low flow rates as ~9 mPa s for the whole saliva sample and ~2 mPa s for the centrifuged samples, close to the values found using the m-VROC rheometer, see Fig. 3. In extensional flow, a small extra pressure is measured due to the macromolecular orientation observed visually through flow-induced birefringence in Fig. 6.

Figure 9a shows the shear and extensional viscosities of the centrifuged 'M' and 'S' saliva samples as a function of the strain rate in the cross-slot, determined from the pressure drop measurements shown in Fig. 8b, measurements of the widths of birefringent regions in Fig. 6 and using Eqs. 3 and 4, respectively. The shear response of both samples was essentially similar, so only one data set is shown for clarity. The slight increase in apparent shear viscosity over the experimental strain rate range of $\sim 100\,\mathrm{s}^{-1} < \dot{\varepsilon} < \sim 3{,}000\,\mathrm{s}^{-1}$ is most likely due to inertial effects in the flow, as shown by the quadratic fit to the pressure drop data in Fig. 8. The extensional viscosity we observe for both of the saliva samples in Fig. 9a shows dramatically different behavior from the shear viscosity. In extension we see a rapid increase in the viscosity from low strain rates up to a maximum value of 0.6–0.7 Pa s at $\dot{\varepsilon} \sim 1{,}200\ \mathrm{s}^{-1}$. Subsequently, with further increase in the strain rate, the extensional

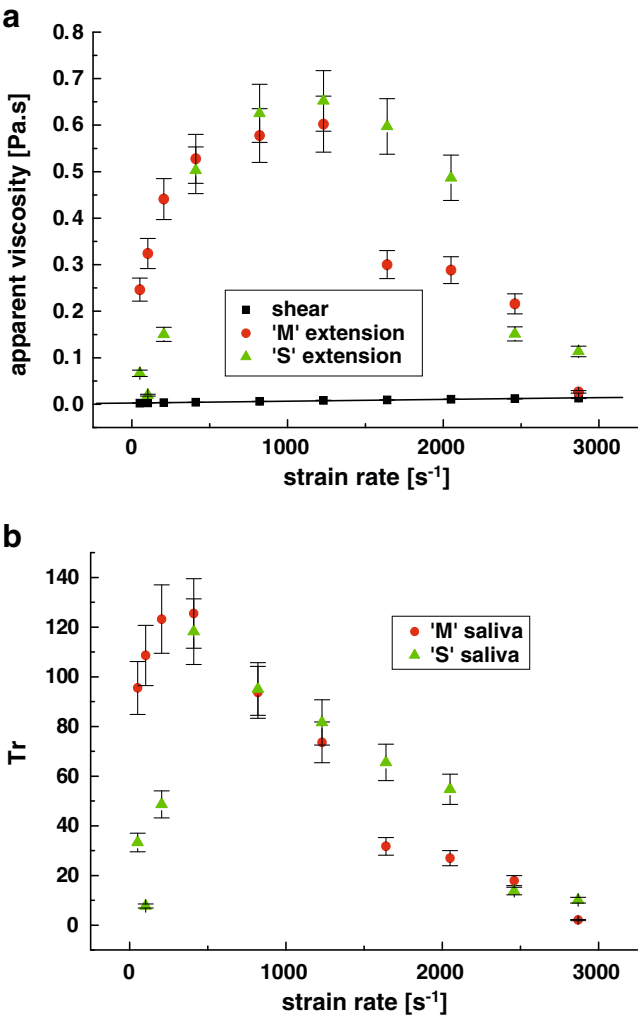

Fig. 9 **a** Apparent viscosity as a function of strain rate for centrifuged human saliva derived from the data shown in Figs. 7b and 5, **b** Trouton ratio as a function of strain rate, determined from the data of (**a**)

viscosity drops again. This high strain rate region corresponds to the broadening of the birefringent strands observed in Fig. 6, which in other studies is associated with significant flow modification along the central axis of the cross-slot (Haward et al. 2010a, b). Inertial effects, breakage of inter-mucin disulfide bonds, and flow-induced scission of high molecular weight mucins may also be significant at such high strain rates.

Figure 9b shows the Trouton ratio, Tr, as a function of strain rate, derived from the data of Fig. 9a according to Eq. 5. The Trouton ratio increases to a maximum value of ∼120–130 at a strain rate of ∼500 s^{-1}, before subsequently reducing. The peak value of Trouton ratio is consistent with values measured with dilute polymer solutions (e.g., Haward et al. 2010a) and demonstrates the significant elasticity of saliva. However, we should expect whole saliva, containing more high molecular weight molecules, to possess an even higher Trouton ratio. Such elasticity may help the saliva to adhere to surfaces within the mouth, thereby serving a protective role as a barrier to acid or microbial attack and helping to prevent build up of plaque and food debris (Campese et al. 2009; Glantz 1997). The coating of the oral cavity by such a shear thinning fluid would also aid lubrication of the mouth to assist actions such as chewing, swallowing, and speech articulation. The altered rheology of soft foods and beverages, due to mixing and interacting with saliva during processing in the mouth, also plays a critical role in sensory perception (Van Aken et al. 2007).

Conclusions

We have demonstrated the capability of a modified EFOR system to quantitatively measure extensional viscosities and flow-induced birefringence with very small quantities of fluid. We have used this ability to make such measurements, for the first time, using samples of human saliva.

The saliva collected from two healthy people, without stimulation, was remarkably similar, qualitatively and quantitatively. Although the saliva had to be centrifuged, which reduces the concentration of mucins, the samples obtained from both donor subjects showed marked non-Newtonian flow effects. A flow-induced birefringent strand was observed along the stagnation point streamline for strain rates above $\dot{\varepsilon} \sim 200\,s^{-1}$, indicating a relaxation time for the longest salivary mucin macromolecules in the sample of $\tau \sim 5$ ms. At higher strain rates significant broadening of the observed birefringence to streamlines passing far from the stagnation point most likely reflects the worm-like nature of the mucins. From birefringence measurements, we have been able to make an initial estimate of the birefringence from a fully stretched salivary mucin to be $\Delta n_0 \sim 0.015$ (although there are caveats placed on this figure).

Viscometry of the saliva samples showed a rapidly increasing extensional viscosity with strain rate, reaching Trouton ratios of up to ∼120, resulting from the highly elastic nature of saliva, although the elasticity of whole saliva would have been underestimated in this study. This high elasticity is likely to be of great importance to saliva functionality in terms of lubrication and surface adhesion within the oral cavity and in binding of the bolus when masticating. It is also an important factor to be considered in the formulation of artificial salivas for the treatment of dry mouth conditions, and is likely to have a significant impact on texture perception in the mouth during processing and consumption of food and drinks.

In addition to continuing our study of saliva rheological properties in the EFOR, we further propose to study the extensional rheology of mucus in asthma and cystic fibrosis, healthy and diseased synovial fluid, and other highly extensible bio-fluids.

Acknowledgements JA Odell and SJ Haward gratefully acknowledge the financial support of the Engineering and Physical Sciences Research Council (EPSRC), UK. We thank professor GH McKinley for the use of his m-VROC rheometer.

References

Backus C, Carrington SP, Fisher LR, Odell JA, Rodrigues DA (2002) The roles of extensional and shear flows of synovial fluid and replacement systems in joint protection. In: Kennedy JF, Phillips OG, Williams PA, Hascall VC (eds) Hyaluronan: chemical, biochemical and biological aspects, vol 1. Woodhead Publishing Ltd., Cambridge, pp 209–218

Beeley JA (1993) Fascinating families of proteins: electrophoresis of human saliva. Biochem Soc Trans 21:133–138

Briedis D, Moutrie MF, Balmer RT (1980) A study of the shear viscosity of human whole saliva. Rheol Acta 19:365–374

Campese M, Sun X, Bosch JA, Oppenheim FG, Helmerhorst EJ (2009) Concentration and fate of histatins and acidic proline-rich proteins in the oral environment. Arch Oral Biol 54:345–353

Carrington SP, Odell JA, Fisher L, Mitchell J, Hartley L (1996) Polyelectrolyte behaviour of dilute xanthan salt effects on extensional rheology. Polymer 37:2871–2875

Carrington SP, Tatham JP, Odell JA, Saez AE (1997a) Macromolecular dynamics in extensional flows: 1. Birefringence and viscometry. Polymer 38:4151–4164

Carrington SP, Tatham JP, Odell JA, Saez AE (1997b) Macromolecular dynamics in extensional flows: 2. The evolution of molecular strain. Polymer 38:4595–4607

Clift AF, Scott-Blair GN (1945) Observations on certain rheological of human cervical secretions. Proc R Soc Med 39:1–9

Colby RH (2010) Structure and linear viscoelasticity of flexible polymer solutions: comparison of polyelectrolyte and neutral polymer solutions. Rheol Acta 49:425–442
Craven TJ, Rees JM, Zimmerman WB (2010) Pressure sensor positioning in an electrokinetic microrheometer device: simulations of shear-thinning liquid flows. Microfluid Nanofluid 9:559–571
Davies JR, Kirkham S, Svitacheva N, Thornton DJ, Carlstedt I (2007) MUC16 is produced in tracheal surface epithelium and submucosal glands and is present in secretions from normal human airway and cultured bronchial epithelial cells. Int J Biochem Cell Biol 39:1943–1954
Davis SS (1971) The rheological properties of saliva. Rheol Acta 10:28–35
Dewar MR, Parfitt GJ (1954) An investigation of the physical properties of saliva and their relationship to the mucin content. J Dent Res 33:596–605
Erbring H (1936) Untersuchungen über die spinnbarkeit flussige systeme. Kolloid-Beihefte 44:171–177
Flory PJ (1969) Statistical mechanics of chain molecules. Interscience, New York
Fox PC, Bodner L, Tabak LA, Levine MJ (1985) Quantitation of total human salivary mucins. J Dent Res 64:327
Glantz P-O (1997) Interfacial phenomena in the oral cavity. Colloids Surf, A 123–124:657–670
Graessley WW (1980) Polymer chain dimensions and the dependence of viscoelastic properties on concentration, molecular weight and solvent power. Polymer 21:258–262
Hattrup CL, Gendler SJ (2008) Structure and function of the cell surface (tethered) mucins. Ann Rev Phys 70:431–457
Haward SJ, Odell JA, Li Z, Yuan X-F (2010a) Extensional rheology of dilute polymer solutions in oscillatory cross-slot flow: the transient behaviour of birefringent strands. Rheol Acta 49:637–645. doi:10.1007/s00397-009-0420-6
Haward SJ, Odell JA, Li Z, Yuan X-F (2010b) The rheology of polymer solution elastic strands in extensional flow. Rheol Acta 49:781–788. doi:10.1007/s00397-010-0453-x
Helmerhorst EJ, Oppenheim FG (2007) Saliva: a dynamic proteome. J Dent Res 86:680–693
Keller A, Müller AJ, Odell JA (1987) Entanglements in semidilute solutions as revealed by elongational flow studies. Prog Colloid Polym Sci 75:179–200
Kesimer M, Sheehan JK (2008) Analysing the functions of large glycoconjugates through the dissipative properties of their absorbed layers using the gel-forming mucin MUC5B as an example. Glycobiology 18:463–472
Kesimer M, Makhov AM, Griffith JD, Verdugo P, Sheehan JK (2010) Unpacking a gel-forming mucin: a view of MUC5B organization after granular release. Am J Physiol Lung Cell Mol Physiol 298:L15–L22
Kratky O, Porod G (1949) Röntgenuntersuchung gelöszer Fadenmoleküle. Rec Trav Chim Pays-Bas 68:1106–1123
Lacombe CH, Essabbah H (1981) Comparative haemorheology of pathological blood. Scand J Clin Lab Investig 41:249–250
Mehrotra R, Thornton DJ, Sheehan JK (1998) Isolation and physical characterization of the MUC7 (MG2) mucin from saliva: evidence for self-association. Biochem J 334:415–422
Odell JA, Carrington SP (2006) Extensional flow oscillatory rheometry. J Non-Newton Fluid Mech 137:110–120
Pedersen AM, Bardow A, Beier Jensen S, Nauntofte B (2002) Saliva and gastrointestinal functions of taste, mastication, swallowing and digestion. Oral Dis 8:117–129
Perkins TT, Smith DE, Chu S (1997) Single polymer dynamics in an elongational flow. Science 276:2016–2021
Rayment SA, Liu B, Offner GD, Oppenheim FG, Troxler RF (2000) Immunoquantification of human salivary mucins MG1 and MG2 in stimulated whole saliva: factors influencing mucin levels. J Dent Res 79:1765–1772
Raynal BDE, Hardingham TE, Thornton DJ, Sheehan JK (2002) Concentrated solutions of salivary MUC5B mucin do not replicate the gel-forming properties of saliva. Biochem J 362:289–296
Riddiford CL, Jerrard HG (1970) Limitations on the measurement of relaxation times using a pulsed Kerr effect method. J Phys D Appl Phys 3:1314–1321
Rossi S, Marciello M, Bonferoni MC, Ferrari F, Sandri G, Dacarro C, Grisoli P, Caramella C (2010) Thermally sensitive gels based on chitosan derivatives for the treatment of oral mucositis. Eur J Pharm Biopharm 74:248–254
Round AN, Berry M, McMaster TJ, Stoll S, Gowers D, Corfield AP, Miles MJ (2002) Heterogeneity and persistence length in human ocular mucins. Biophys J 83:1661–1670
Rubin BK (2007) Mucus structure and properties in cystic fibrosis. Paediatr Respir Rev 8:4–7
Schipper RG, Silletti E, Vingerhoeds MH (2007) Saliva as research material: biochemical, physicochemical and practical aspects. Arch Oral Biol 52:1114–1135
Schwarz WH (1987) The rheology of saliva. J Dent Res 66:660–666
Scrivener O, Berner C, Cressely R, Hocquart R, Sellin R, Vlachos NS (1979) Dynamical behaviour of drag-reducing polymer solutions. J Non-Newton Fluid Mech 5:475–495
Sharma V, Jaishankar A, Wang Y-C, McKinley GH (2010) Rheology of globular proteins: apparent yield stress, high shear rate viscosity and interfacial viscoelasticity of bovine serum albumin solutions. Biophysical J
Sheehan JK, Howard M, Richardson PS, Longwill T, Thornton DJ (1999) Physical characterization of a low-charge glycoform of the MUC5B mucin comprising the gel-phase of an asthmatic respiratory mucous plug. Biochem J 338:507–513
Smith DE, Chu S (1998) Response of flexible polymers to sudden elongational flow. Science 281:1335–1340
Stokes JR, Davies GA (2007) Viscoelasticity of human whole saliva collected after acid and mechanical stimulation. Biorheology 44:141–160
Thomsson KA, Prakobphol A, Leffler H, Reddy MS, Levine MJ, Fisher SJ, Hansson GC (2002) The salivary mucin MG1 (MUC5B) carries a repertoire of unique oligosaccharides that is large and diverse. Glycobiology 12:1–14
Thornton DJ, Khan N, Mehrotra R, Howard M, Veerman E, Packer NH, Sheehan JK (1999) Salivary mucin MG1 is comprised almost entirely of different glycosylated forms of the MUC5B gene product. Glycobiology 9:293–302
Treloar LKG (1975) The physics of rubber elasticity, 3rd edn. Clarendon, Oxford
Van Aken GA, Vingerhoeds MH, de Hoog EHA (2007) Food colloids under oral conditions. Curr Opin Colloid Interface Sci 12:251–262
Van der Reijden WA, Veerman ECI, Amerongen AVN (1993a) Shear rate-dependent viscoelastic behaviour of human glandular salivas. Biorheology 30:141–152
Van der Reijden WA, Veerman ECI, Amerongen AVN (1993b) Erratum: shear rate-dependent viscoelastic behaviour of human glandular salivas. Biorheology 30:301
Waterman HA, Blom C, Holterman HJ, 's-Gravenmade EJ, Mellema J (1988) Rheological properties of human saliva. Arch Oral Biol 33:589–596
Zussman E, Yarin AL, Nagler RM (2007) Age- and flow-dependency of salivary viscoelasticity. J Dent Res 86:281–285